Expanded View Figures

Figure EV1. Validation of temperature-dependent AS in mammalian cells.

A Principle component analysis of the investigated triplicate samples by RNA sequencing.

B Distribution of splicing types in events identified to change after CHX treatment. AA alternative acceptor, AD alternative donor, AF alternative first exon, AL alternative last exon, CE cassette exon, RI retained intron, TE transcription end, TS transcription start.

C Overlap of genes with CHX-dependent events identified in our study in primary mouse hepatocytes (34 and 38°C) and by Hurt *et al*., 2013 in embryonic stem cells (37°C).

D Number of alternative cassette exons that have a stop codon included, grouped by whether and how the exons are alternatively spliced upon CHX treatment. ****$P < 0.0001$, Chi-square test.

E Automatic cluster mapping of temperature-dependent splicing changes in CHX, based on PSI (percent spliced in). All events with $|\Delta PSI| > 0.15$ and $P > 0.85$ between CHX 34 and 38°C are shown. $N = 4{,}740$.

F, G In (F), examples for heat-skipped (white) or cold-skipped (gray) splicing events. Note that these splicing events are barely affected by CHX. In (G), further examples for cold-induced (blue) or heat-induced (red) AS-decay events. Box plots show median PSI of validation PCRs of four different samples from at least two different mice, whiskers show min to max. Individual data points are shown as circles. Statistical significance was determined by two-way ANOVA and is indicated by asterisks: adjusted *P* values: not significant (ns), *$P < 0.05$, **$P < 0.01$, ***$P < 0.001$, ****$P < 0.0001$.

H Comparison of temperature-regulated AS events predicted by Whippet RNA-Seq analysis and validated by RT–PCR from independent samples. The line depicts linear regression; goodness of fit is indicated by R^2.

I Comparison of splicing changes in CHX (*x*-axis) and DMSO (*y*-axis) for all events presented in EV1E. The line depicts linear regression, goodness of fit is indicated by R^2, $N = 4{,}740$. The *P* value represents statistical probability of the slope being different from 0. Splicing changes in DMSO and CHX have the same directionality but ΔPSI values are generally larger in CHX.

J Temperature dependence of the strongest decay events (top 500, largest ΔPSI in either 34 or 38°C comparison of DMSO vs CHX). Categories (right) were manually assigned. We define four categories: (i) cold-induced decay, (ii) heat-induced decay, (iii) temperature-independent decay, and (iv) CHX-sensitive temperature-dependent splicing events. The generation of these isoforms could depend on *de novo* protein synthesis.

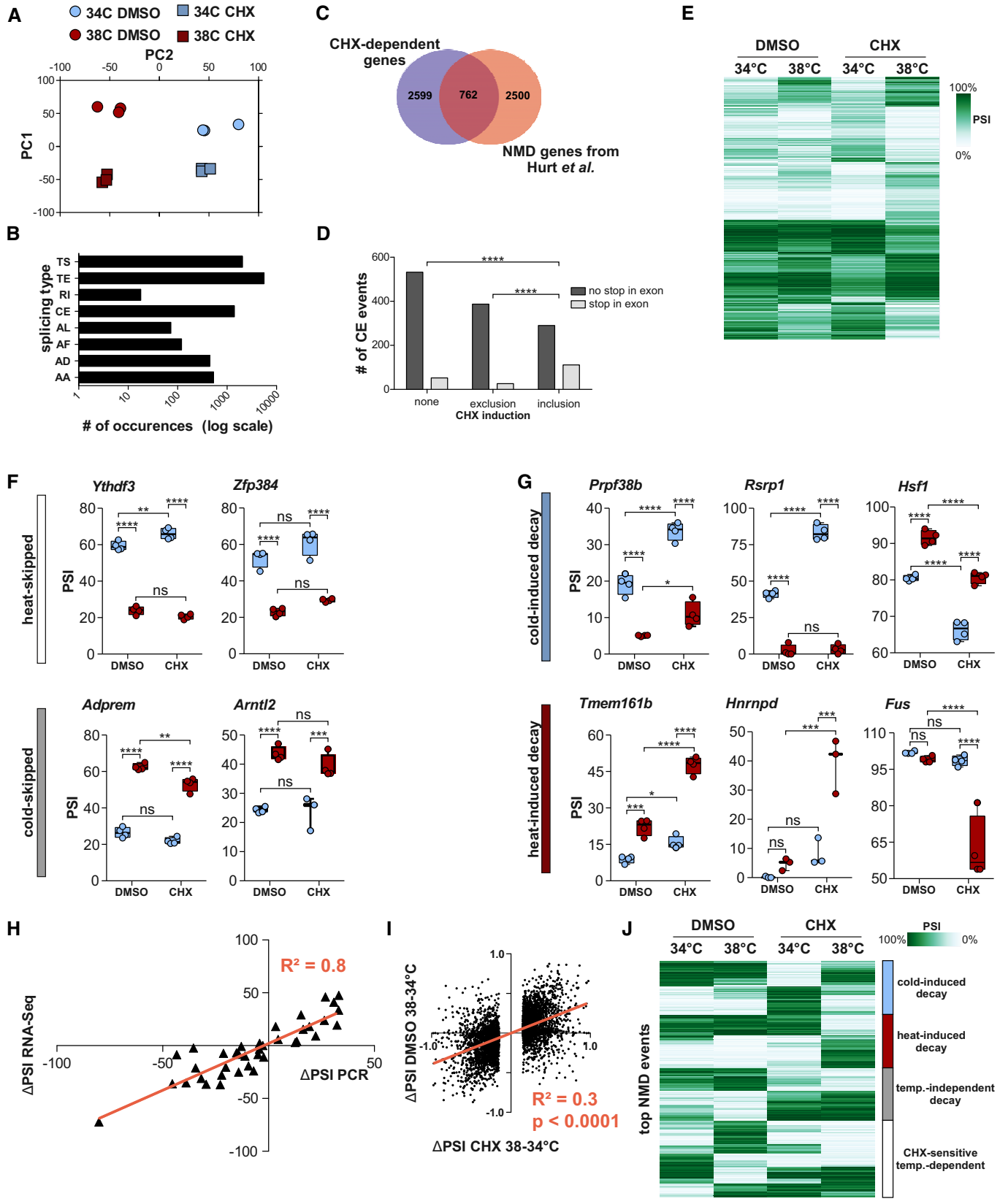
A
34C DMSO
34C CHX
38C DMSO
38C CHX
PC2
PC1
B
splicing type
TS
TE
RI
CE
AL
AF
AD
AA
# of occurences (log scale)
C
CHX-dependent genes
2599
762
2500
NMD genes from Hurt et al.
D
# of CE events
no stop in exon
stop in exon
none
exclusion
inclusion
CHX induction
E
DMSO
CHX
34°C
38°C
PSI
100%
0%
F
heat-skipped
Ythdf3
Zfp384
cold-skipped
Adprem
Arntl2
PSI
DMSO
CHX
G
cold-induced decay
Prpf38b
Rsrp1
Hsf1
heat-induced decay
Tmem161b
Hnrnpd
Fus
H
ΔPSI RNA-Seq
ΔPSI PCR
R² = 0.8
I
ΔPSI DMSO 38-34°C
ΔPSI CHX 38-34°C
R² = 0.3
p < 0.0001
J
top NMD events
cold-induced decay
heat-induced decay
temp.-independent decay
CHX-sensitive temp.-dependent

Figure EV1.

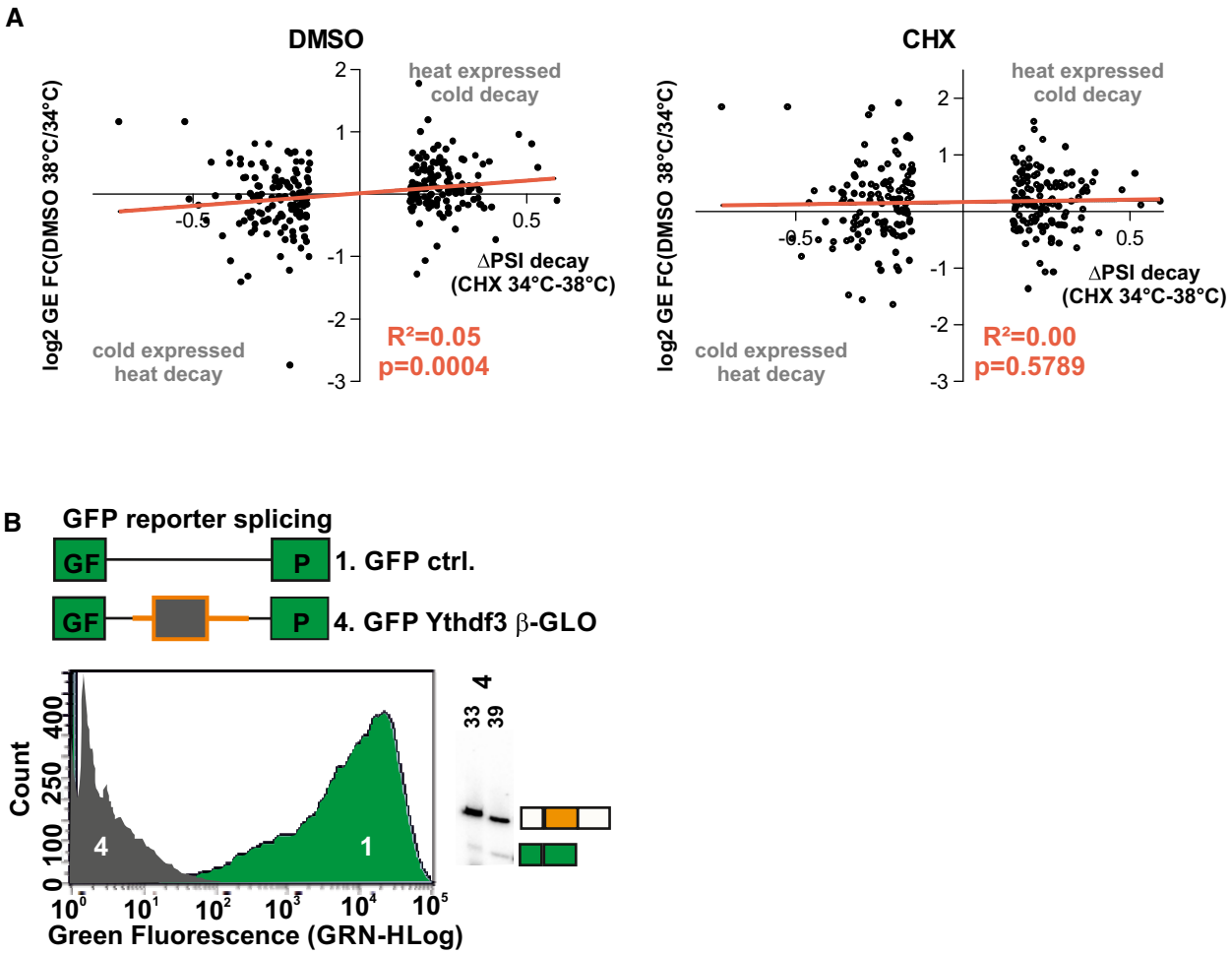

Figure EV2. Temperature-dependent poison events globally regulate GE.

A Global correlation of poison isoform inclusion and GE levels for all genes with temperature-dependent AS-decay skipped exon events. Shown are the $\log_2$ fold change (FC) in GE vs the ΔPSI of the poison isoform between the CHX samples. Left shows the GE change between the DMSO samples and right the between the CHX samples at the two temperatures. R^2 and P (deviation from zero slope) are indicated, $N = 254$.

B Exon inclusion abolishes the GFP signal. Replacing the central 27 nucleotides of exon 7 in the Ythdf3 reporter (GFP Ythdf3 b-GLO, #4) results in almost complete exon inclusion (RT–PCR, bottom right). A cytometric analysis comparing this mutant (#4, > 95% exon inclusion) and the GFP ctrl (#1, almost complete skipping) confirms that exon inclusion abolishes the GFP signal.

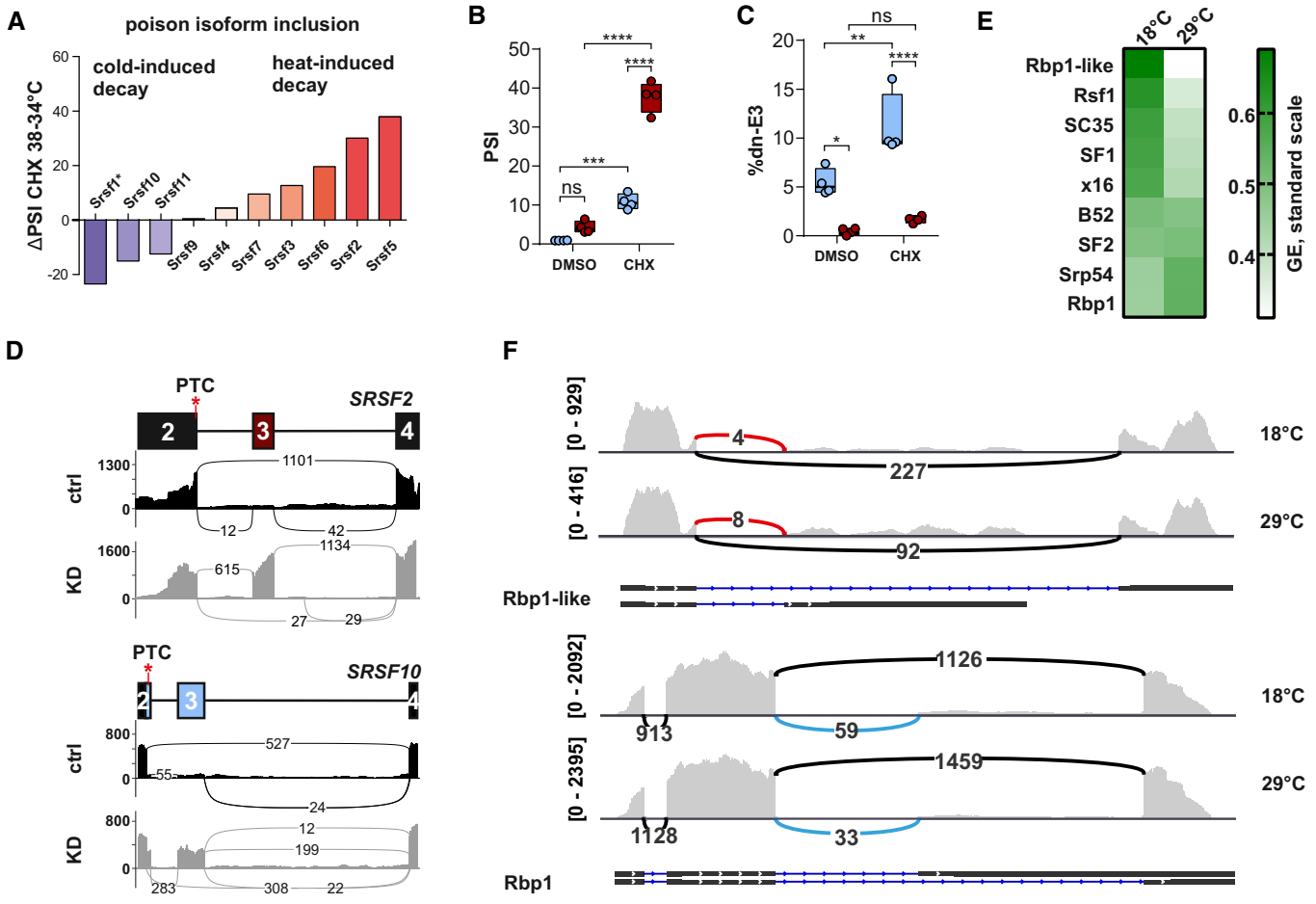

Figure EV3. Temperature-dependent AS-decay is evolutionary-conserved.

A Comparing temperature-dependent AS-decay (ΔPSI of 38–34°C in CHX) of SR proteins in primary mouse hepatocytes. The poison event in *Srsf1* (*) escaped the computational analysis; data are derived from radioactive RT–PCR.

B Validation of *Srsf2* temperature-dependent AS-decay by radioactive RT–PCR as described in Fig 1C. Box plots show median PSI of validation PCRs of four different samples from at least two different mice; whiskers show min to max. Individual data points are shown as circles. Statistical significance was determined by two-way ANOVA and is indicated by asterisks: adjusted *P* values: not significant (ns), ***$P < 0.001$, ****$P < 0.0001$.

C Validation of *Srsf10* temperature-dependent AS-decay by radioactive RT–PCR as described in (A). Box plots show median PSI of validation PCRs of four different samples from at least two different mice; whiskers show min to max. Individual data points are shown as circles. Statistical significance was determined by two-way ANOVA and is indicated by asterisks: adjusted *P* values: not significant (ns), *$P < 0.05$, **$P < 0.01$, ****$P < 0.0001$.

D Sashimi plots for SRSF2 (top) and SRSF10 (bottom) confirming increased poison exon inclusion upon SMG6/SMG7 double KD (light gray) compared to control (black).

E Heatmap for SR protein expression in *D. melanogaster*. Normalized mean GE in ovaries kept at 18 or 29°C ($n = 2$, (Fast *et al*, 2017)) is shown for each SR protein. Note cold-induced expression of the SRSF2 homolog SC35.

F Sashimi plots indicating heat-induced (red, top) or cold-induced (blue, bottom) generation of a low-abundance splicing isoform in cold-induced Rbp1-like (top) or heat-induced Rbp1 (bottom).

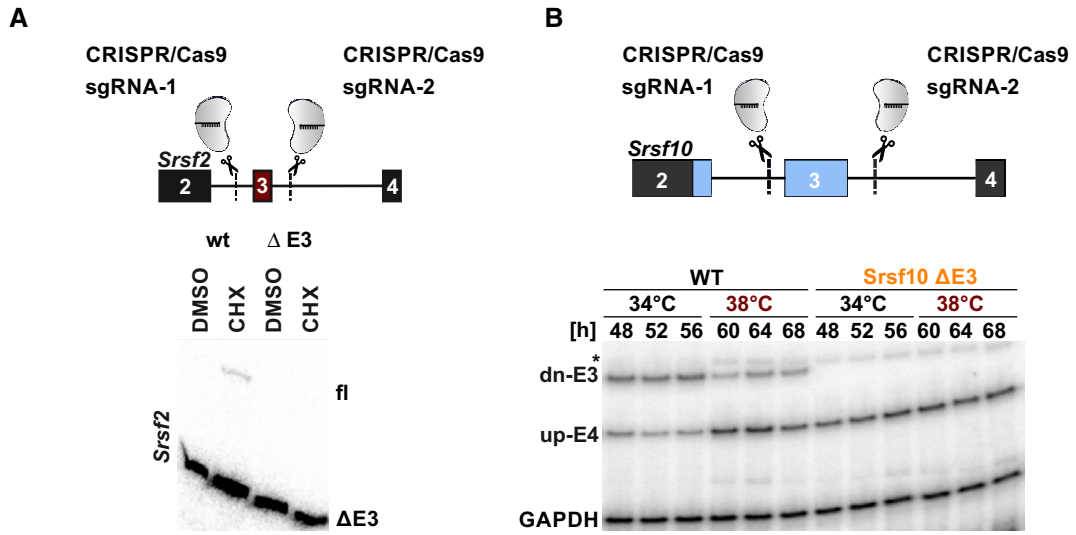

Figure EV4. Temperature-dependent AS-decay is necessary for rhythmic GE.

A, B CRISPR/Cas9 strategy for cell lines lacking poison exons for *Srsf2* (A) and *Srsf10* (B). Lack of poison exons in clonal *Srsf2* CRISPR/Cas9-edited cell lines was confirmed by splicing sensitive RT–PCR (bottom). WT and mutant cell lines were treated with DMSO or CHX at 38°C and inclusion of the poison isoform was investigated by splicing sensitive RT–PCR (A). Investigation of *Srsf10* dn-E3 splicing in samples from Fig 4C. AS was analyzed by RT–PCR. A *Gapdh* PCR was performed simultaneously and served as a loading control. A representative gel image is shown. The asterisk indicates an unspecific product.

Figure EV5. Temperature-dependent AS-decay of SR proteins in plants and in mice.

A Normalized poison isoform expression of plant SR proteins as in Fig 5A. In this dataset, without inhibition of decay pathways, the identification of poison isoforms is likely incomplete (compare to B). In three cases, a clear temperature-regulated alternative polyadenylation (APA) event occurred but was not quantified (also indicating a post-transcriptional origin of temperature-dependent GE). In two cases, no poison event could be identified. Four times decay seemed to be too efficient, as no poison isoform could be identified without CHX treatment.

B Poison isoform inclusion in WT- or CHX-treated plants for the same genes as in (A). Here, the amount of the respective isoforms was compared in control and CHX-treated samples (based on another RNA-Seq dataset (Drechsel *et al*., 2013), see Table EV1). Note that most temperature-dependent isoforms from (A) are stabilized upon CHX treatment.

C Validation RT–PCRs and qPCRs of poison events in further plant SR proteins as shown in Fig 5D. For each case, poison isoform inclusion correlates with lower GE. Lines represents mean.

D Validation of an AS-decay event in GEMIN2, in which cold-induced inclusion of the poison isoform correlates with lower GE. Lines represents mean.

E Correlation of rhythmic productive *Srsf10* mRNA expression (orange, left *y*-axis) and exon 3 inclusion (black, right *y*-axis) in mouse cerebellum samples from the indicated ZTs. Splicing was analyzed using radioactive RT–PCR of at least three mice per time point. Expression was determined by RT–qPCR and is shown relative to *Hprt* and ZT0 (mean of at least three mice ± SEM). Student's unpaired *t*-test-derived *P* values $^{**}P < 0.01$, $^{***}P < 0.001$ indicate difference from ZT0.

F Rhythmic *Srsf10* AS persists in constant darkness. Mice were kept in constant darkness for 24 h and sacrificed at the indicated circadian times (CTs) of the following subjective day. RT–PCR analysis as in (A) ($n = 3$, median ± min to max). Student's unpaired *t*-test-derived *P* values $^{*}P < 0.05$.

G Entrained *Srsf10* AS. Mice were 8-h phase delayed and sacrificed at the indicated ZTs on the 4th day. RT–PCR analysis as in (A) ($n = 3$, median ± min to max). Student's unpaired *t*-test-derived *P* values $^{*}P < 0.05$.

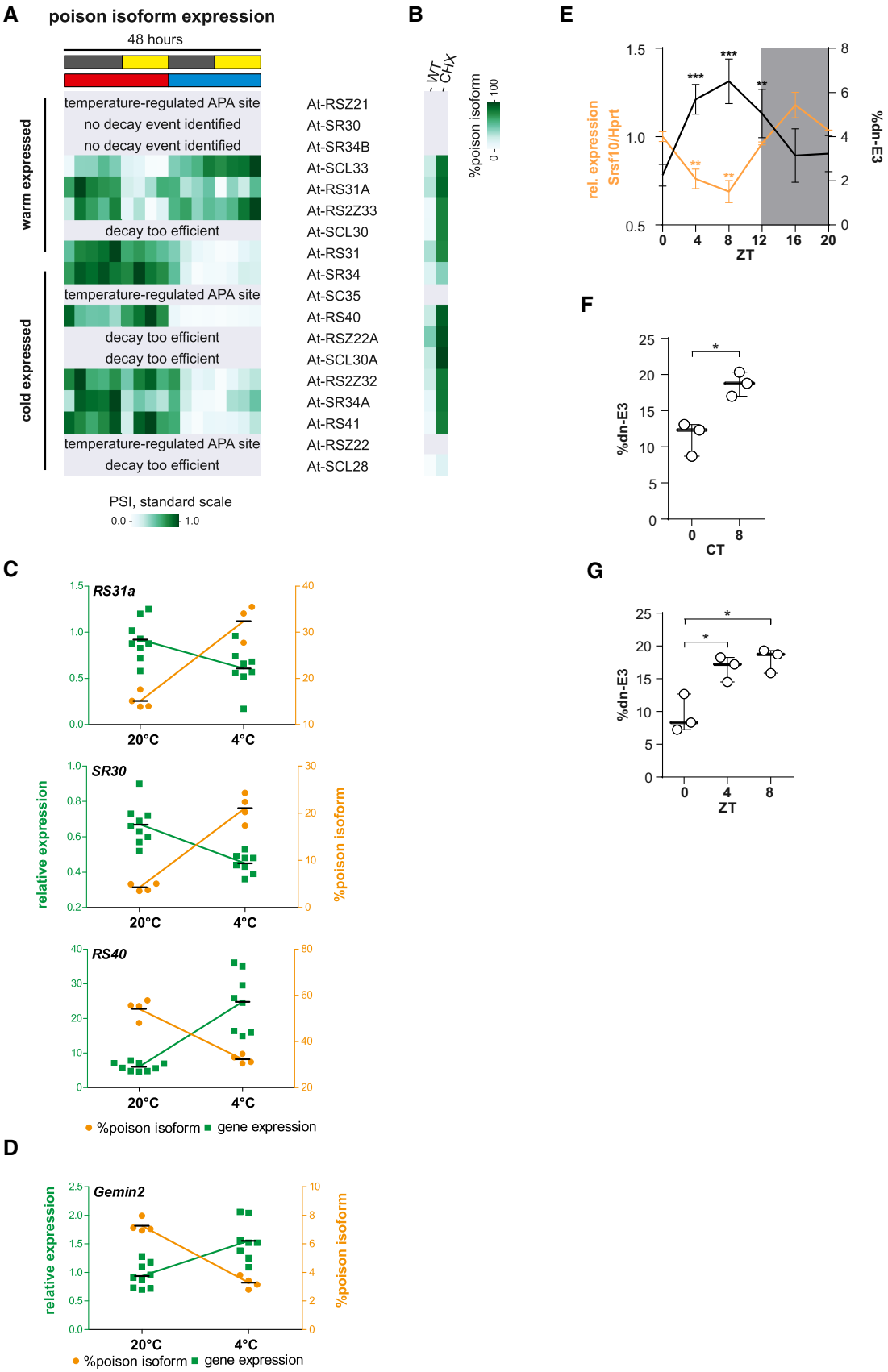
A
poison isoform expression
48 hours
warm expressed
cold expressed
temperature-regulated APA site
no decay event identified
no decay event identified
decay too efficient
temperature-regulated APA site
decay too efficient
decay too efficient
temperature-regulated APA site
decay too efficient
At-RSZ21
At-SR30
At-SR34B
At-SCL33
At-RS31A
At-RS2Z33
At-SCL30
At-RS31
At-SR34
At-SC35
At-RS40
At-RSZ22A
At-SCL30A
At-RS2Z32
At-SR34A
At-RS41
At-RSZ22
At-SCL28
PSI, standard scale
0.0
1.0
B
WT
CHX
%poison isoform
100
0
E
rel. expression Srsf10/Hprt
%dn-E3
ZT
F
%dn-E3
CT
G
%dn-E3
ZT
C
RS31a
SR30
RS40
relative expression
%poison isoform
20°C
4°C
%poison isoform
gene expression
D
Gemin2
relative expression
%poison isoform
20°C
4°C
%poison isoform
gene expression

Figure EV5.